

Wavefield resampling during Kirchhoff extrapolation

Gary F. Margrave and Hugh D. Geiger

ABSTRACT

Recursive Kirchhoff wavefield extrapolators can be used to both downward-continue a digital seismic wavefield and to interpolate it to new spatial locations. We present a brief review of the Kirchhoff theory and then three numerical experiments, in 2D, intended to demonstrate the capabilities of the Kirchhoff extrapolators. In the first two experiments the input wavefield is a 256 trace synthetic wavefield computed by upward extrapolating two impulses in a laterally variable velocity using the exact wavefield extrapolation theory. In a first test, the input wavefield is decimated to 128 regularly spaced traces and a reconstruction is attempted of the initial wavefield while downward extrapolating the decimated wavefield. This is compared to a downward extrapolation of the full 256 trace wavefield. The reconstructed wavefield is very similar to the full wavefield except for a slight increase in noise. The spectrum of the reconstructed wavefield has been extended beyond the spatial Nyquist for 128 traces; however, energy that was aliased in the decimation was not unaliased. This leads to the increased noise. A second test is similar except that the original 256 trace wavefield was downsampled to 162 traces chosen at random. Again a good reconstruction is obtained characterized by tight focusing plus noise. However, the noise is not easily attributable to aliased energy this time. Finally, a real shot record is used with results that are consistent with the conclusions obtained from synthetics. The recursive Kirchhoff approach is postulated to be especially useful for extrapolation of data acquired at irregular locations.

INTRODUCTION

Last year we presented a development of Kirchhoff wavefield extrapolation (Margrave and Daley, 2001). Beginning with the Fourier integral operator expressions for the wavefield extrapolators: NSPS (*nonstationary phase shift*), GPSPI (*generalized phase shift plus interpolation*), and the Weyl operator (based upon a quantum mechanical idea in Weyl (1931)) (see Margrave and Ferguson, 1998, 1999, and Ferguson and Margrave 2001), expressions were derived for all three extrapolators in the space-frequency domain. As might be expected, these expressions turned out to be Kirchhoff-style operators that accomplish a single wavefield extrapolation step rather than a complete migration. The only difference between the three operators, NSPS, GPSPI, and Weyl, was found to be in the way they handle velocity (more on this below) and the computational cost was found to be the same for each and is independent of the velocity complexity. The more conventional approach of deriving Kirchhoff wavefield extrapolators from the Kirchhoff integral is discussed in Kuhn and Alhilali (1977) Schneider (1978), Berryhill (1979, 1984), Berkhout (1981, 1985), and (Wiggins (1984). Good overviews can be found in Bevc (1995, 1997) and Geiger (2002).

Kirchhoff integral expressions are more familiar in the context of a complete Kirchhoff migration than as wavefield extrapolators, so it is worth discussing the distinction. In Kirchhoff migration, any point in the image volume is computed as a weighted summation through the input data volume along a traveltime surface. This

traveltime surface is defined by raytracing from the image point to each source and receiver location. In the constant velocity case, the traveltime surface is a hyperboloid in 3D and a hyperbola in 2D. Though all points in the image volume are computed in a similar fashion, in general each point has a unique summation curve. The computation of these summation curves is a major component of the algorithm and effectively limits the image to energy that has propagated along Snell's law raypaths. In contrast, Kirchhoff wavefield extrapolation is not a complete imaging calculation but must be used in a recursive wavefield marching scheme, together with an imaging condition, to achieve a migration. A single step of a Kirchhoff wavefield extrapolation is also a weighted summation along a traveltime surface but that surface is invariant in time, and for constant velocity, is also invariant in space. This means that Kirchhoff wavefield extrapolation is a multidimensional convolution that is possibly nonstationary in the lateral spatial coordinates if velocity varies laterally. In our approximate extrapolators, there is no need for explicit raytracing because only straight rays are used so the summation surface can be calculated analytically. In the case of NSPS, the traveltimes are computed using the velocity at the input points (i.e. the beginning of the raypaths) as shown in Figure 1. Figure 2 shows the case for GPSPI which computes the traveltimes using the velocity at the output points (the end points of the raypaths). Finally, the Weyl extrapolator (Figure 3) uses the average of the velocity at the beginning and end of each raypath. As with any recursive extrapolation scheme, the final image point is formed from data that has moved along all possible paths not just the Snell's law raypath.

The Kirchhoff wavefield extrapolators have many features in common with their Fourier integral counterparts including fast and accurate adaptation to lateral velocity variations. In fact, all of these extrapolators are superior in accuracy to any finite-difference or phase-screen operators. The Kirchhoff extrapolators are fairly expensive to compute but their cost is purely a function of the data size and is completely independent of the complexities of the velocity model. In contrast, the Fourier integral operators have very low cost for constant velocity and, for random velocity, are more expensive than the Kirchhoff operators.

A key feature of the Kirchhoff wavefield extrapolators, and the subject of this paper, is that the input and output data geometries are not directly coupled. In contrast, Fourier or finite-difference methods have strong computational and accuracy incentives for identical input and output geometries. This strength of the Kirchhoff extrapolators makes them very attractive for land surveys with irregular geometry. A reasonable expectation is that Kirchhoff wavefield extrapolators will allow irregular acquisition geometries to be regularized in the first few downward continuation steps. Once the geometry has been regularized, then it is very reasonable to switch to Fourier extrapolators, or any other form, if computational efficiencies can be gained. In the next section we demonstrate this *geometry changing* feature of the Kirchhoff wavefield extrapolators on synthetic and real data.

THEORY REVIEW

We consider wavefield extrapolation with the 2D Kirchhoff implementation of the GPSPI extrapolator (Margrave and Daley, 2001). If $\psi(x, z = 0, \omega)$ is a wavefield in the

space-frequency (x, ω) domain at depth level $z = 0$, then its value at depth z is estimated as

$$\psi_{GPSPI}(x, z, \omega) = -i \frac{\omega}{v(x)} \int_{-\infty}^{\infty} \psi(\hat{x}, z=0, \omega) \cos(\theta) H_1^{(1)}\left(\frac{\omega \rho}{v(x)}\right) d\hat{x} \quad (1)$$

where the integration is over the input lateral coordinate, \hat{x} , θ is the scattering angle, $v(x)$ is the laterally variable velocity, $H_1^{(1)}$ is the first order Hankel function of the first kind, and the 2D radius vector, ρ , is given by

$$\tilde{\rho} = \sqrt{(x - \hat{x})^2 + z^2}. \quad (2)$$

The scattering angle is simply the angle that a ray makes with respect to the vertical (see Figures 1, 2, and 3) and is defined by

$$\cos(\theta) = \frac{z}{\rho}. \quad (3)$$

Margrave and Daley (2001) also give an approximate form for equation (1) using a large-argument approximation for the Hankel function but we have found that the exact form is needed. We implemented our code in MATLAB where the Hankel functions are provided with the function *besselh*.

Equation (1) is a type of *nonstationary convolution* because the Hankel function argument depends upon both the spatial difference, $x - \hat{x}$, and directly upon x through the lateral velocity variation. Since the spatial summation involved in (1) is precisely prescribed for all x , not just those on a particular grid, the output geometry is effectively decoupled from the input. That is, we can estimate the extrapolated wavefield at lateral positions that are distinct from those of the input wavefield. In particular, as in the case of most land acquisition, an irregular geometry can perhaps be *interpolated* to a regular one. A key question is to ask what are the properties of this interpolation.

While highly effective, equation (1) is still only an approximation to the exact expression. Margrave et al. (2002) show that the exact wavefield extrapolator in the 2D, discretely-sampled case, can be written as

$$\psi(x, z, \omega) = F_{k_x \rightarrow x}^{-1} \left(\underline{\underline{U}} \left\{ \underline{\underline{U}}^{-1} \left(F_{\hat{x} \rightarrow k_x} \left[\psi(\hat{x}, z=0, \omega) \right] \right) e^{i\sqrt{\lambda}z} \right\} \right), \quad (4)$$

where F is the discrete Fourier transform, $\underline{\underline{U}}$ is the eigenvector matrix for the matrix $\underline{\underline{M}}$ defined by

$$\underline{\underline{M}} = - \begin{bmatrix} k_{x0}^2 & & & 0 \\ & k_{x1}^2 & & \\ & & \ddots & \\ 0 & & & k_{xn}^2 \end{bmatrix} + \omega^2 \begin{bmatrix} \hat{s}_0 & \hat{s}_{-1} & \cdots & \hat{s}_{-n} \\ \hat{s}_1 & \hat{s}_0 & \hat{s}_{-1} & \\ \vdots & \hat{s}_1 & \ddots & \\ \hat{s}_n & & & \hat{s}_0 \end{bmatrix}, \quad (5)$$

where the elements \hat{s}_k of the Toeplitz matrix on the right are the DFT of $v^{-2}(\hat{x})$. Equation (4) contains a phase-shift operator $\exp(i\sqrt{\underline{\lambda}z})$ where $\underline{\lambda}$ is the vector of eigenvalues of $\underline{\underline{M}}$.

NUMERICAL EXPERIMENTS

We begin by showing results from a synthetic dataset. Figure 4 shows an input wavefield that was upward extrapolated 50 m using the exact 2D algorithm of equation (4). All downward extrapolations in this paper were done with the GPSPI implementation of equation (1). The velocity model is simply 2000 m/s on the left and 3000 m/s on the right with a vertical interface in the precise centre. Figure 5 shows the resulting exact extrapolation. The wavefields in Figures 4 and 5 contain 256 traces. To test the geometry changing feature, we downsampled the exact extrapolation of Figure 5 by simply throwing away every other trace as shown in Figure 5. We hope to be able to downward extrapolate this wavefield at the same time as we restore the missing traces. Figures 7 and 8 are the (k_x, f) magnitude spectra of Figures 5 and 6 respectively. Figure 7 also shows the evanescent boundaries for the two velocities, 2000 m/s and 3000 m/s, and the new Nyquist wavenumber that will result after downsampling. For frequencies below 80 Hz, the only wavelike energy that is greater than the new Nyquist is also evanescent with respect to 3000 m/s. This means that we expect the aliasing induced by downsampling to be associated with the left side of the wavefield. In Figure 8, the aliasing induced by wavefield desampling is quite obvious though it should be noticed that the horizontal axis is expanded relative to Figure 7.

The goal in this first experiment is to downward extrapolate 50 m the wavefield of Figure 5, that has 128 traces, and create a 256 trace output dataset. This will be compared to a direct downward extrapolation of the full wavefield of Figure 4. Figure 9 is the result of downward extrapolating the 128 trace wavefield which simultaneously resampling it to 256 traces. It is apparent that both diffraction hyperbolae have focused but the one on the left, in slower velocity, is surrounded by aliased energy as expected. Figure 10 is the result of a downward extrapolation of the full wavefield of Figure 5. It is interesting to note that the size of the focal points in Figure 9 are the same as in Figure 10, the difference is simply aliased noise. Figures 11, and 12 show the (k_x, f) magnitude spectra of Figures 9 and 10 respectively. Figure 11 shows that the Kirchhoff operator has extended the wavenumber spectrum of the downsampled wavefield beyond its Nyquist wavenumber but the aliased energy remains. This suggests that the interpolation is better than can be done by a Fourier-based, or sinc function, interpolator. While such interpolators can be shown to be optimal for band-limited data, they can never extend the spectrum beyond its Nyquist bounds as has been accomplished here.

To conclude this first example, we show in Figure 13 the 50m upward extrapolation of the wavefield of Figure 6. Effectively, by downward extrapolation with resampling followed by upward extrapolation, we have interpolated the downsampled wavefield back to 256 traces. The interpolation is quite good except for the aliased energy on the left.

For our second example, we consider the effects of random downsampling. In Figure 14, the wavefield of Figure 5 has been downsampled to 162 traces by selecting 94 traces at random for deletion. Figure 15 is the result of a 50 m downward continuation of this randomly downsampled wavefield while simultaneously resampling to 256 traces. Now, unlike the previous example, there are artefacts associated with each focal point. However, the sizes of the focal points are the same as in the best case (Figure 10). Figure 16 shows the restored wavefield created by upward extrapolation of the focused wavefield of Figure 15. This result is definitely inferior to the result from the previous example (Figure 13) but still quite good. In Figure 17, we show the (k_x, f) magnitude spectrum of the wavefield of Figure 15. In comparison with Figure 11, here we see no obvious aliasing artefacts but instead a general mismatch in comparison with the exact result (Figure 12).

Finally, we show a real data example using a Blackfoot shot record (Figure 18). This same shot record is shown in Figure 19 with every other trace deleted. As a comparison, we downward extrapolated both the original shot record and the desampled one through 5 steps of 50 m each using a constant velocity of 2000 m/s. In the desampled case, the geometry was changed on the first step from the desampled case to the fully sampled case. A comparison of Figures 20 and 21 shows the two downward extrapolated wavefields to be quite similar.

CONCLUSIONS

Recursive Kirchhoff wavefield extrapolation in the (x, ω) domain has a formulation that effectively decouples the input and output wavefield geometries. That is, for any output point, the desired result is a weighted summation through the input data along an easily calculated path. The choice of output points is apparently arbitrary though the performance of the resulting interpolation is a strong function of the data geometries. We find that an interpolation from a regular grid to another one with half the grid interval is easily accomplished. In this mode the input wavenumber spectrum is extended beyond the input Nyquist wavenumber as might be expected from a sophisticated dip-steered technique. However, energy aliased on the original grid is not unaliased but remains as noise. We also find that interpolation from a random to a regular geometry is possible though it seems likely that better results will occur when the numbers of input and output points are similar. In particular, we showed an interpolation from 162 random positions to 256 regular positions that is quite promising. Finally, a single test with a real shot record produced results that are consistent with our examination of synthetic data.

RESEARCH PLANS

We intend to implement this geometry changing wavefield extrapolation in 3D in our parallel wavefield extrapolation facility. At that point, we will examine its performance on real datasets.

ACKNOWLEDGEMENTS

Funding for this work came from CREWES, POTSI, NSERC, and MITACS and we thank all of these organizations.

REFERENCES

- Berkhout, A.J., 1981, Wave field extrapolation techniques in seismic migration, a tutorial: *Geophysics*, **46**, 1638-1656
- Berkhout, A.J., 1985, Seismic Migration: Imaging of Acoustic Energy by Wavefield Extrapolation: A: Theoretical Aspects: Elsevier Science Publ. Co., Inc., *Developments in Solid Earth Geophysics*, **14A**.
- Berryhill, J.R., 1979, Wave-equation datuming: *Geophysics*, **44**, 1329-1344.
- Berryhill, J.R., 1984, Wave equation datuming before stack (short note): *Geophysics*, **49**, 2064-2067.
- Bevc, D., 1995, Imaging under Rugged Topography and Complex Velocity Structure: Ph.D. Thesis, Stanford University.
- Bevc, D., 1997, Flooding the topography: Wave-equation datuming of land data with rugged acquisition topography: *Geophysics*, **62**, 1558-1569.
- Ferguson, R.J. and Margrave, G.F., 2001, Prestack depth imaging by symmetric nonstationary phase shift: *Geophysics*, *in press*.
- Geiger, H.D., 2001, Relative-Amplitude-Preserving Prestack Time Migration by the Equivalent Offset Method: Ph.D. Thesis, University of Calgary, 382p.
- Kuhn, M.J. and Alhilali, K.A., 1977, Weighting factors in the construction and reconstruction of acoustical wave fields: *Geophysics*, **42**, 1183-1198.
- Margrave, G.F. and Ferguson, R.J., 1998, Explicit Fourier wavefield extrapolators: CREWES Research Report, Vol. **10**.
- Margrave, G.F. and Ferguson, R.J., 1999, Wavefield extrapolation by nonstationary phase shift: *Geophysics*, **64**, 1067-1078.
- Margrave, G.F., Lamoureux, M.P., Gibson, P.C., Bale, R.A., and Grossman, J.P., 2002, Exact wavefield extrapolation in 2D for $v(x)$: CREWES Research Report, Vol. **14**.
- Schneider, W.A., 1978, Integral formulation for migration in two dimensions or three dimensions: *Geophysics*, **43**, 49-76.
- Weyl, H., 1931, *The Theory of Groups and Quantum Mechanics*: Dover edition (pub 1950).

FIGURES

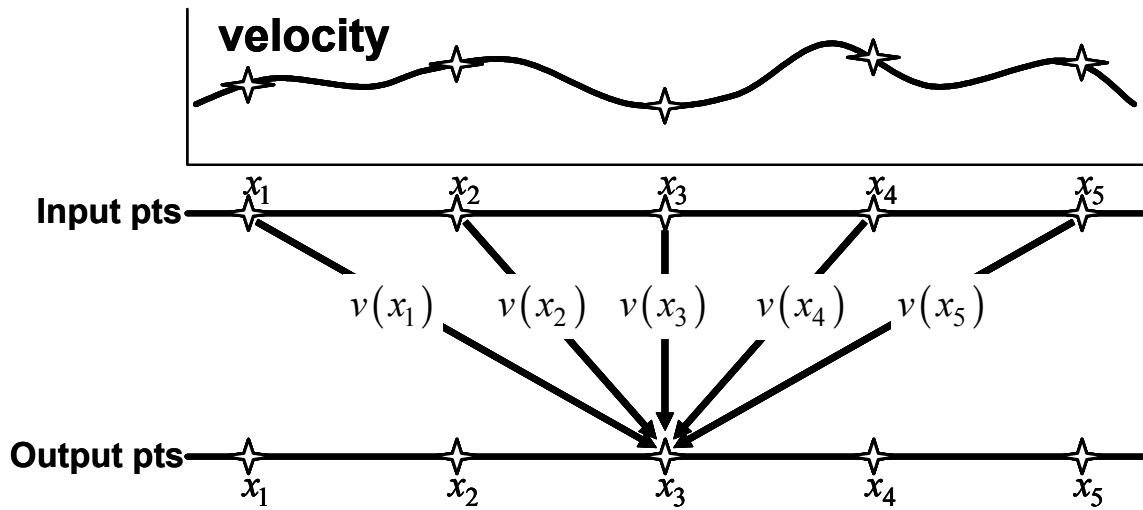


FIG. 1: NSPS wavefield extrapolation calculates a single output point using straight raypaths from each input point and the velocity at the input points.

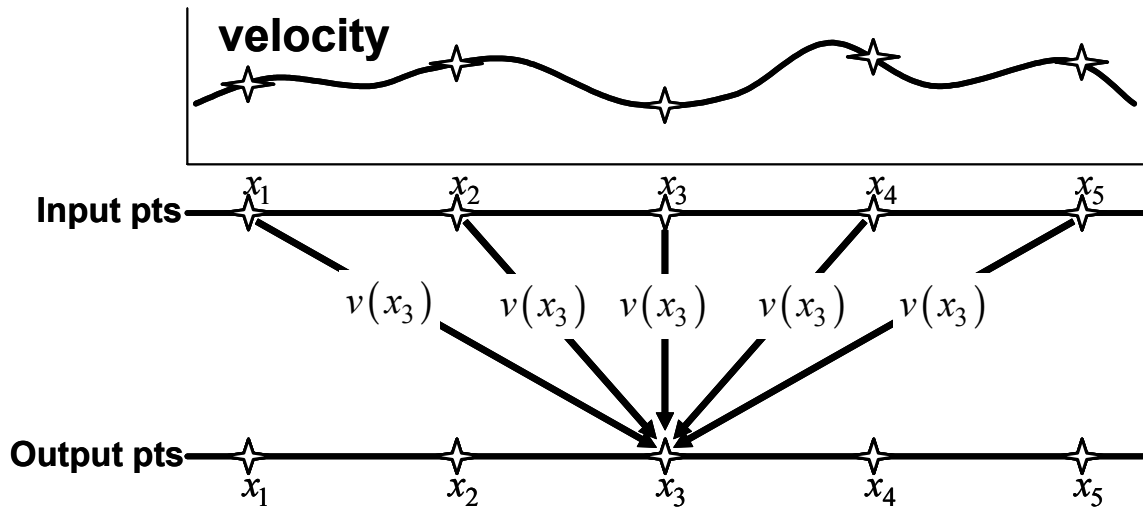


FIG. 2: GPSPI wavefield extrapolation calculates a single output point using straight raypaths from each input point and the velocity at the output point.

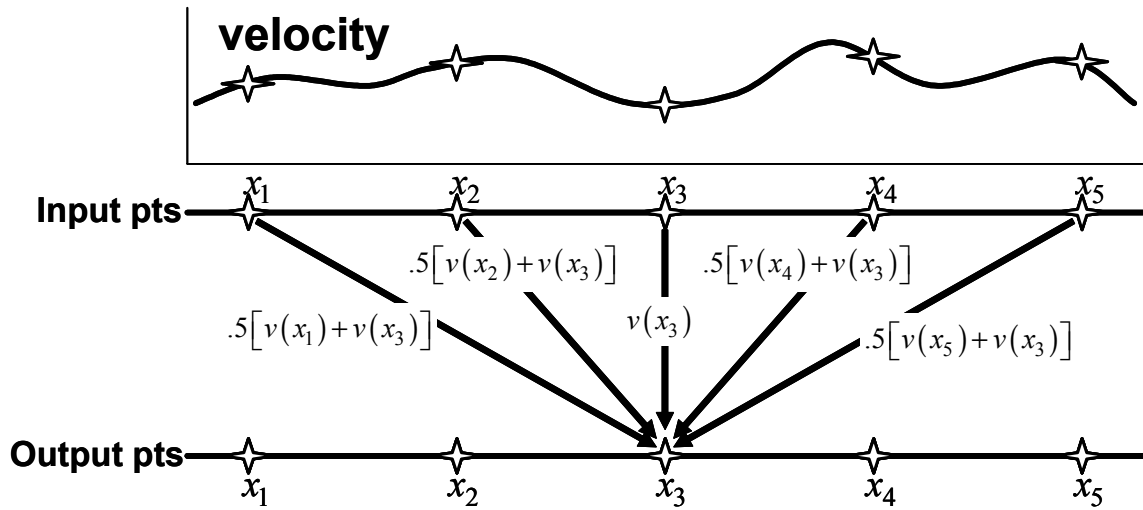


FIG. 3: Weyl wavefield extrapolation calculates a single output point using straight raypaths from each input point and the average of the velocity at the input and output points.

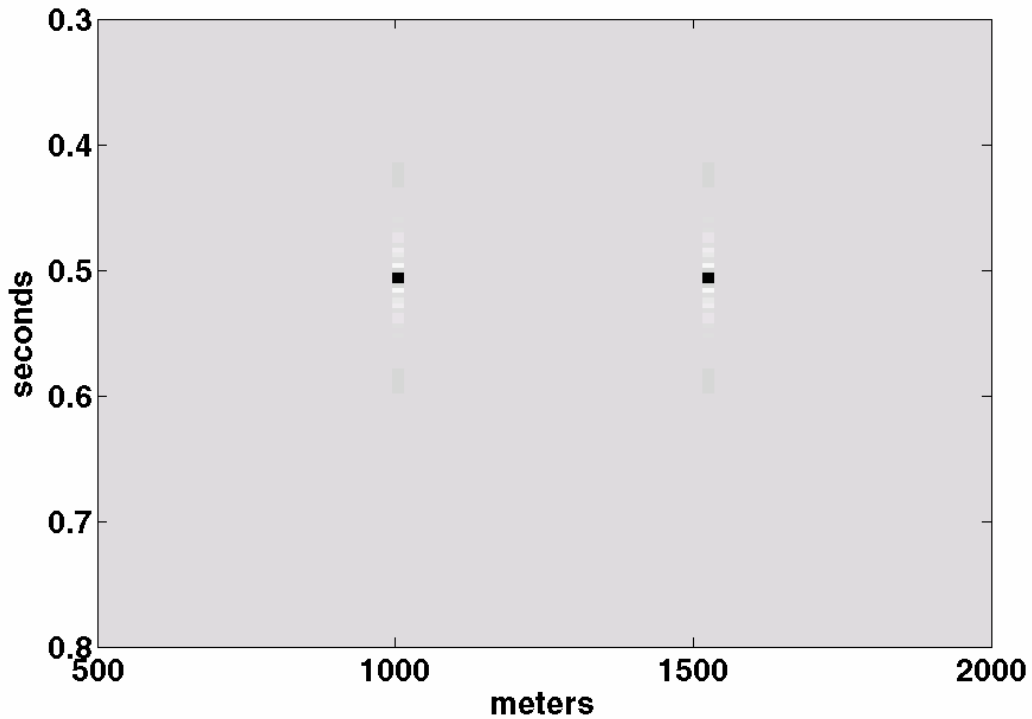


FIG. 4: The Input wavefield for the following series of synthetic experiments. The velocity model has a vertical interface at 1250 m with 2000 m/s on the left and 3000 m/s on the right.

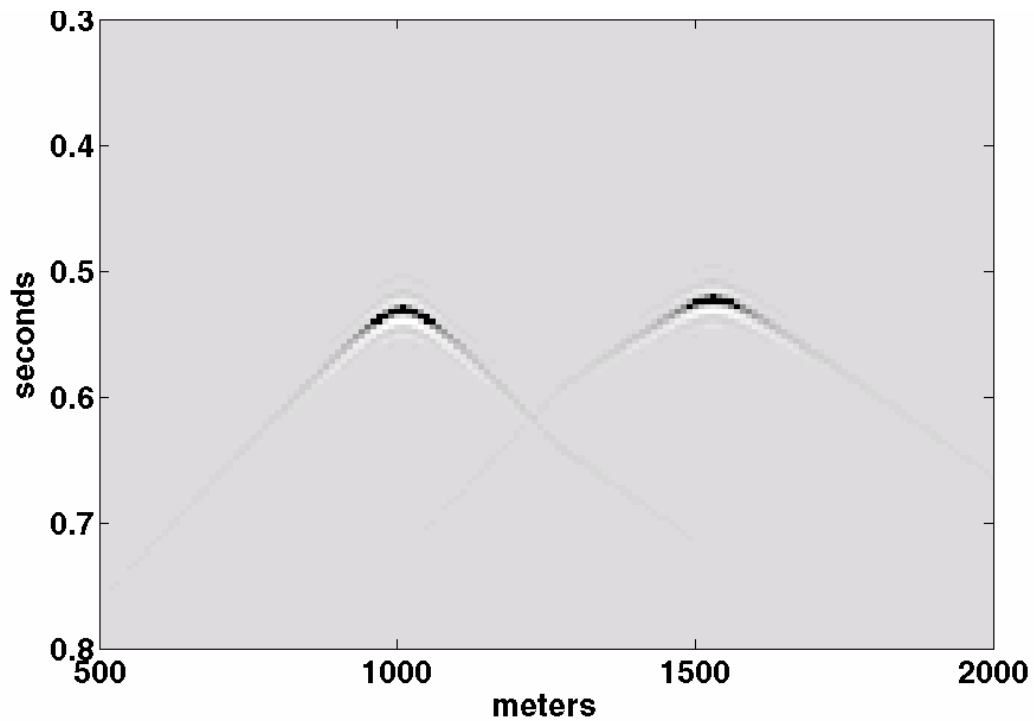


FIG. 5: The result of a 50-metre upward extrapolation of the wavefield of Figure 4 through a bimodal velocity model with 2000 m/s on the left and 3000 m/s on the right. There are 256 traces in this dataset.

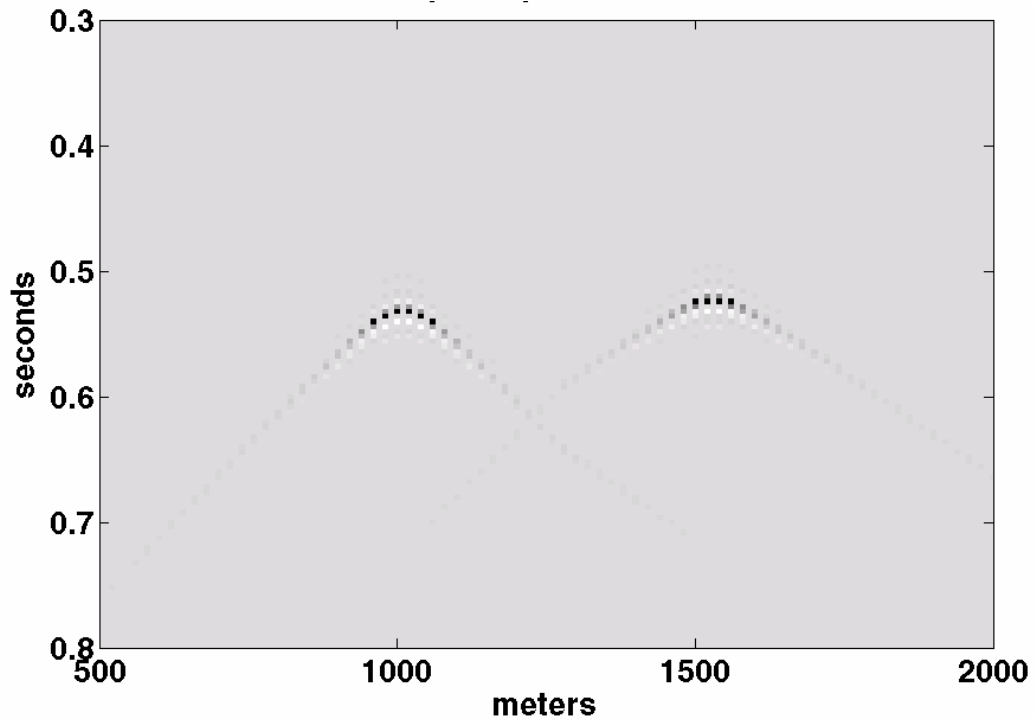


FIG. 6: The wavefield of Figure 5 is shown with every other trace deleted. (Delete traces are shown zero'd for clarity.) There are 128 traces in this dataset.

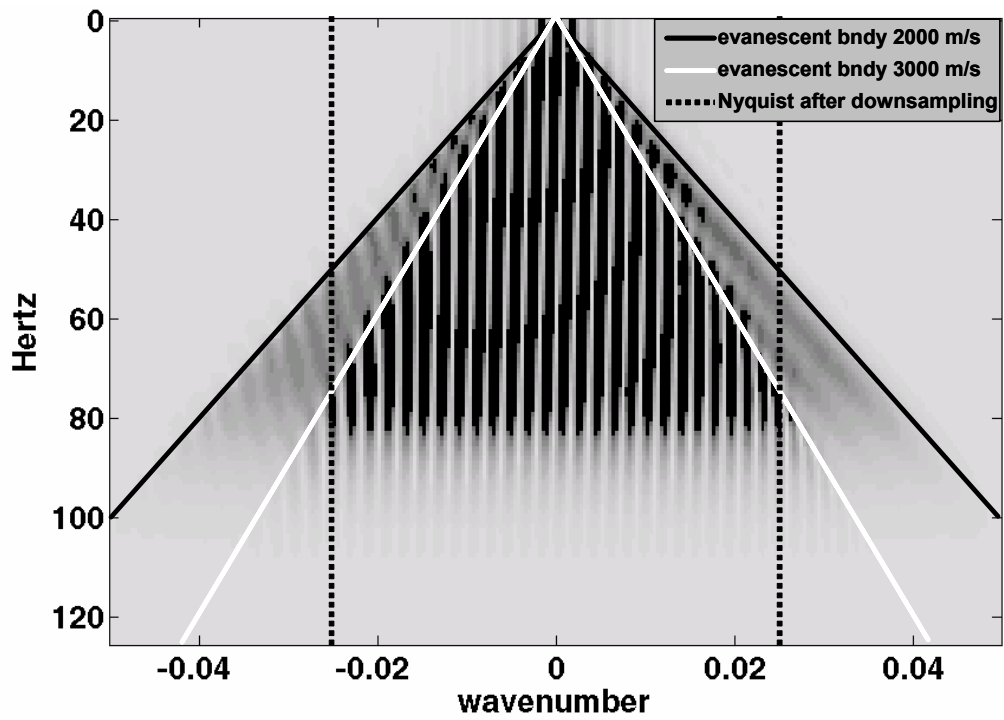


FIG. 7: The (k_x, f) magnitude spectrum of the wavefield of Figure 5.

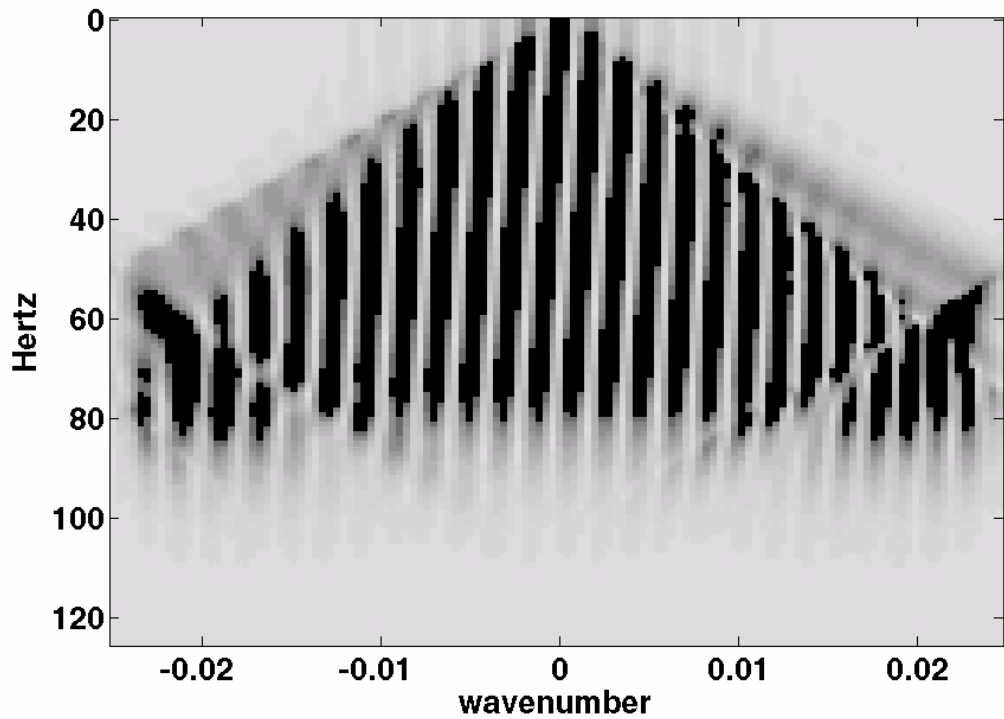


FIG. 8: The (k_x, f) magnitude spectrum of the wavefield of Figure 6.

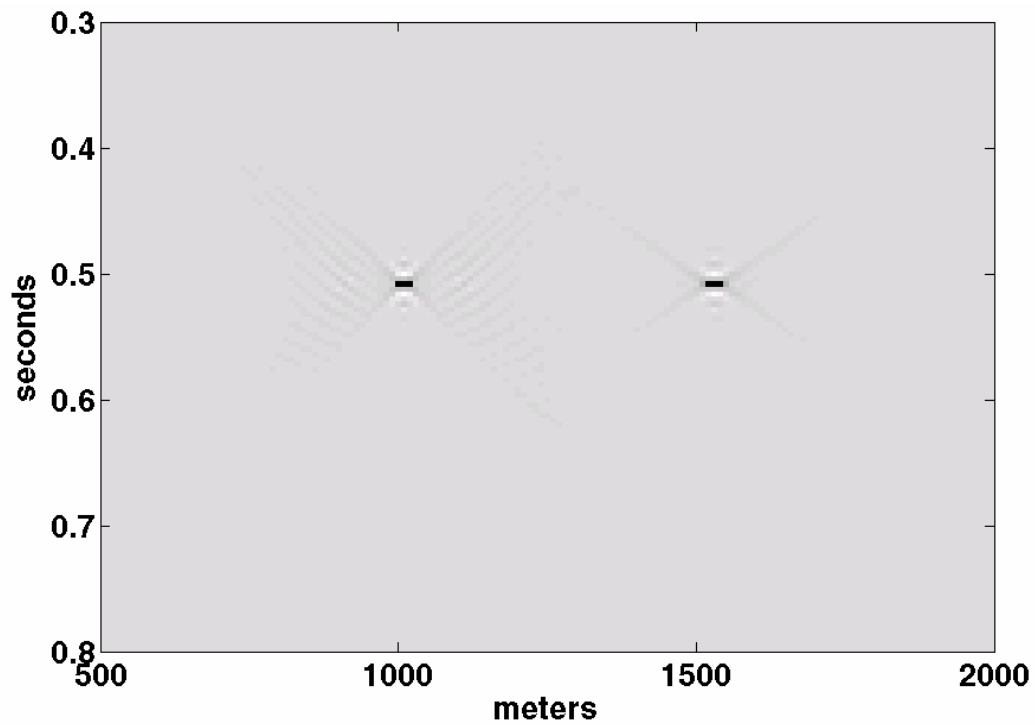


FIG. 9: The result of a 50 m downward extrapolation of the wavefield of Figure 6, that contains only 128 traces, where the output geometry was that of Figure 5 (256 traces).

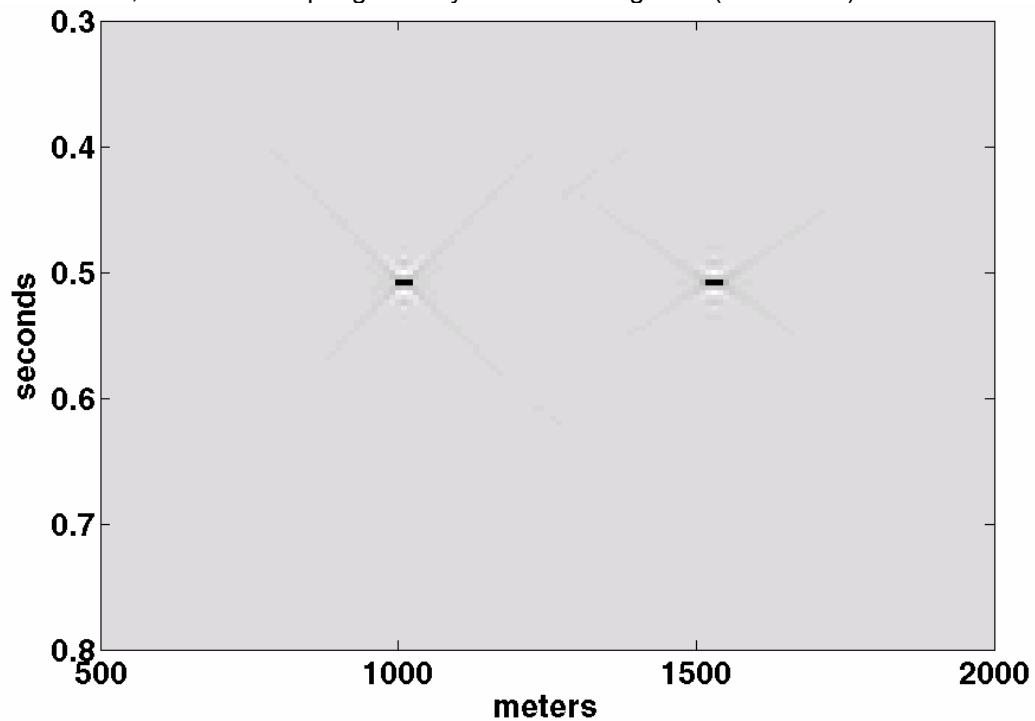


FIG. 10: The result of a 50 m downward extrapolation of the wavefield of Figure 5. Both the input and output geometries included 256 traces. Compare with Figure 9.

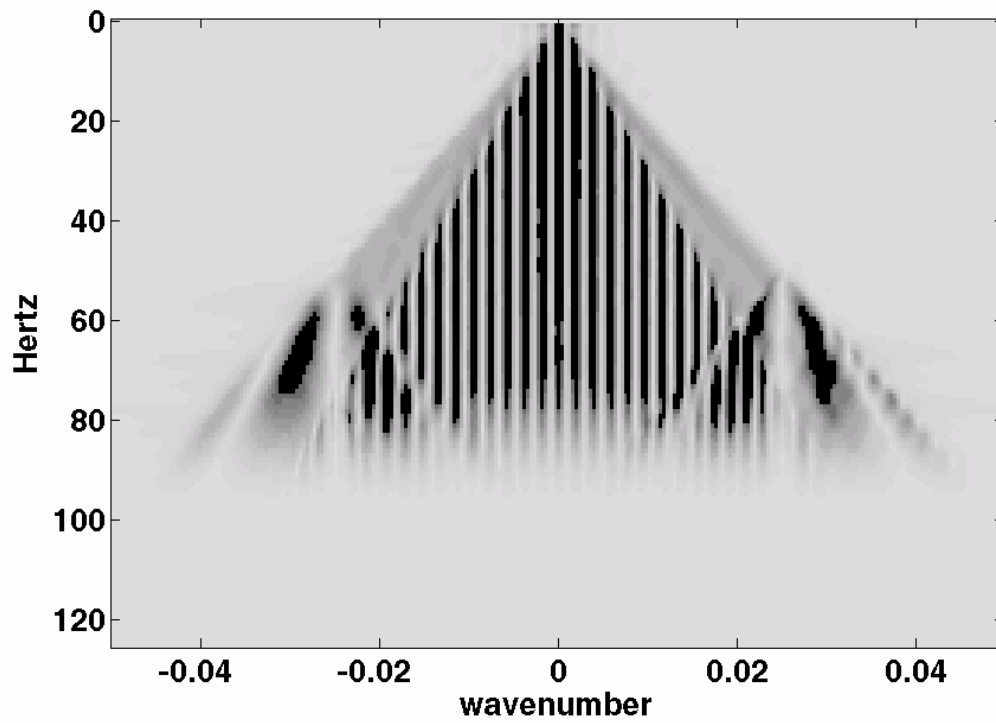


FIG. 11: The (k_x, f) magnitude spectrum of the wavefield of Figure 9.

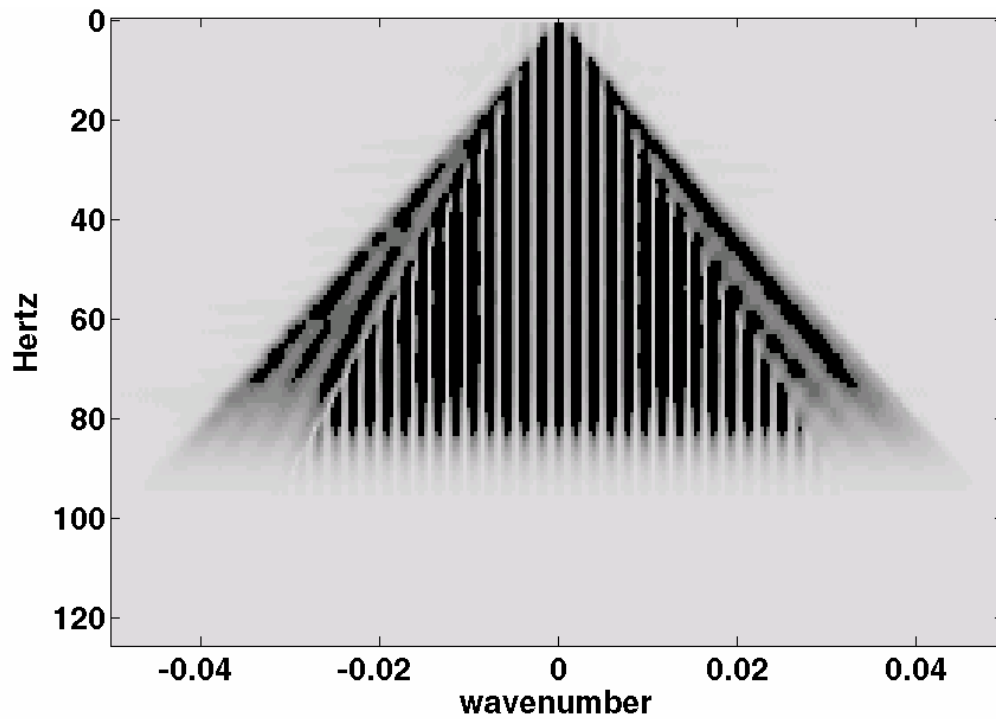


FIG. 12: The (k_x, f) magnitude spectrum of the wavefield of Figure 10.

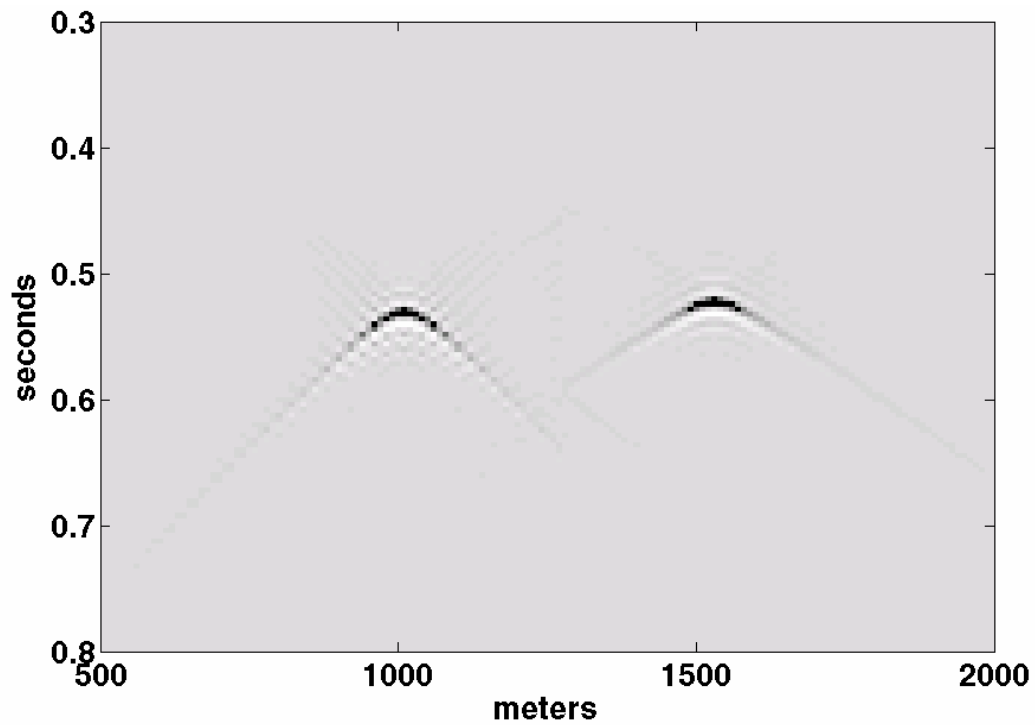


FIG. 13. The wavefield of Figure 9 has been upward extrapolated 50 m to effectively resample the wavefield of Figure 6 back to 256 traces.

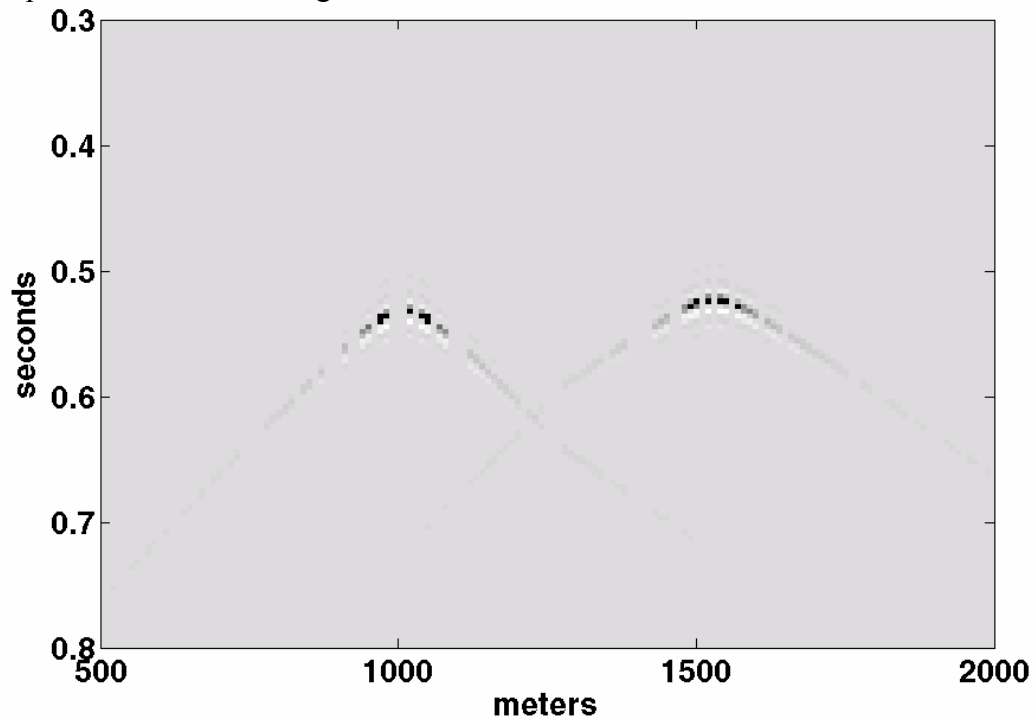


FIG. 14: A 162 trace subset of the wavefield of Figure 5 created by selecting 94 traces at random and deleting them.

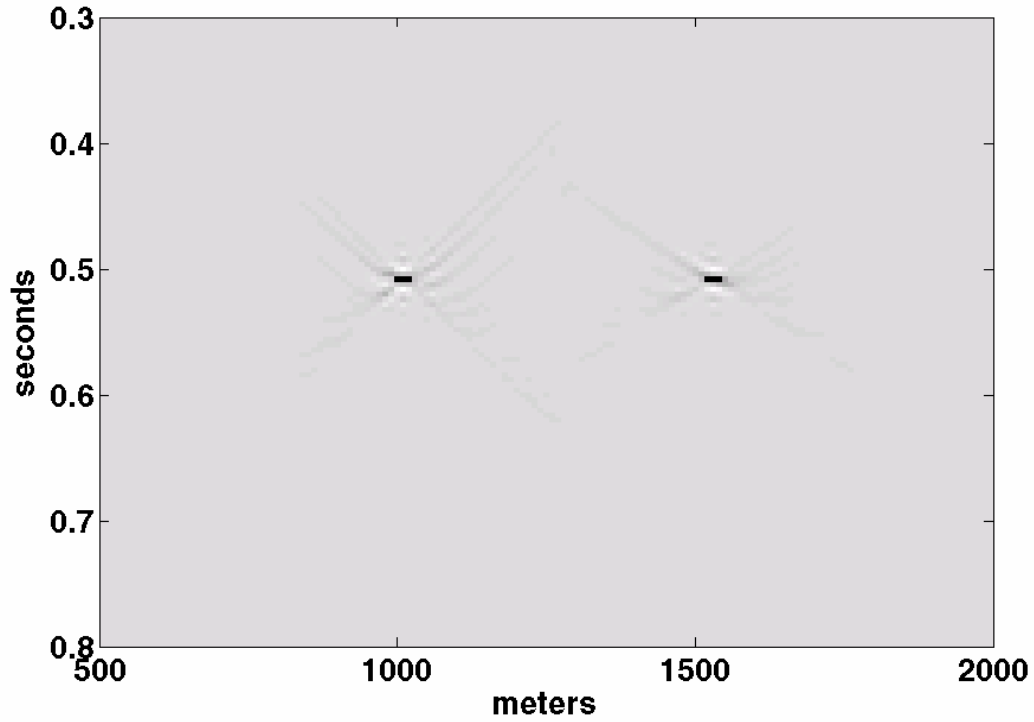


FIG. 15: The wavefield of Figure 14 has been downward extrapolated 50 m and resampled to 256 traces.

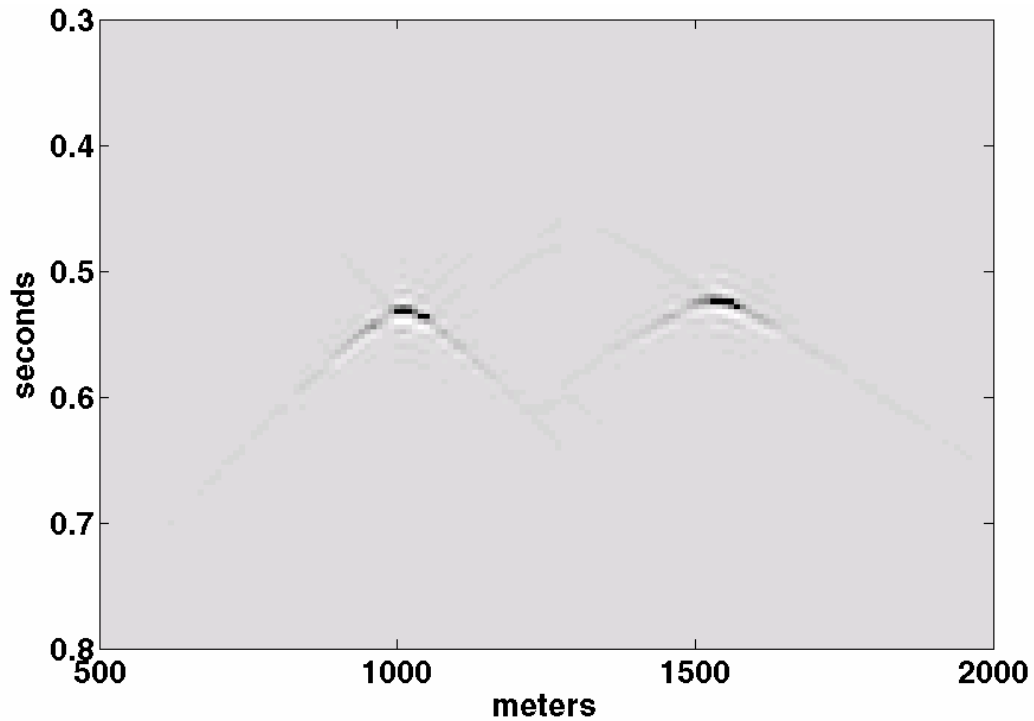


FIG. 16: The wavefield of Figure 15 has been upward extrapolated 50 m to effectively interpolate the randomly downsampled wavefield back to 256 traces. In this case, the interpolation has not filled all of the holes in the wavefield.

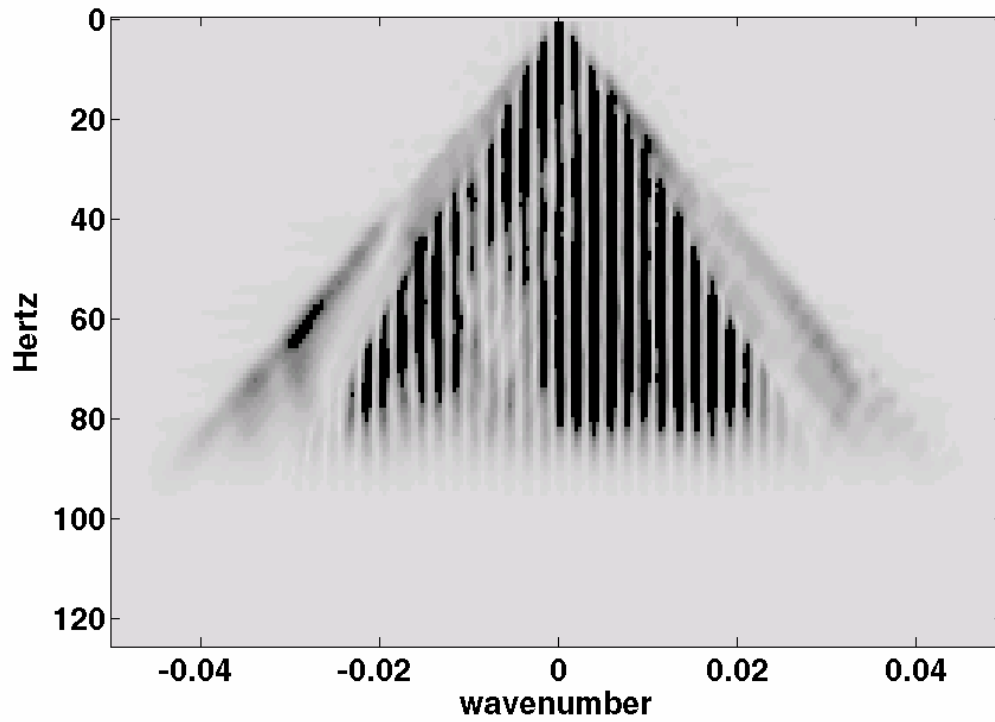


FIG. 17: The (k_x, f) magnitude spectrum of the wavefield of Figure 15.

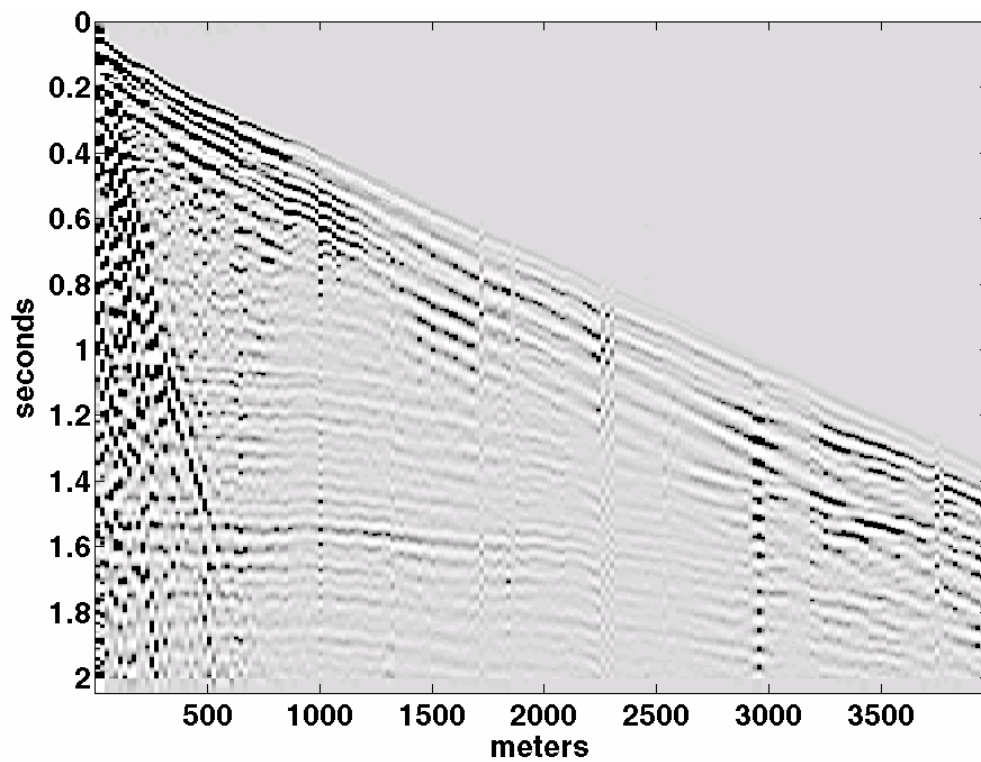


FIG. 18: A shot record from one of the CREWES Blackfoot experiments.

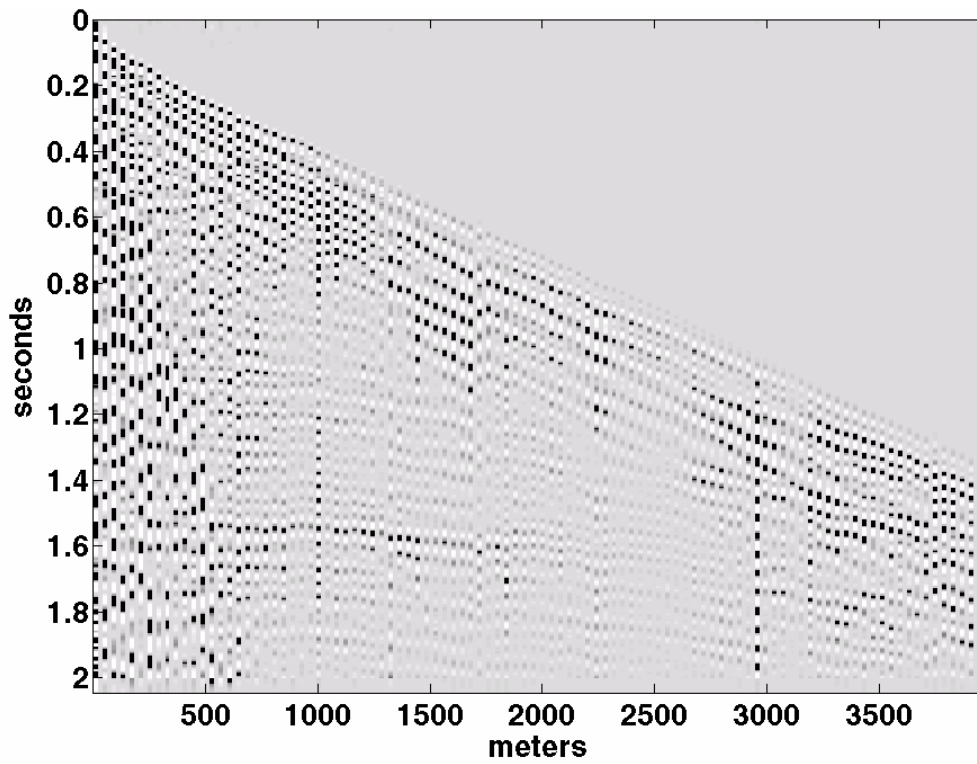


FIG. 19: The shot record of the previous figure with every other trace deleted.

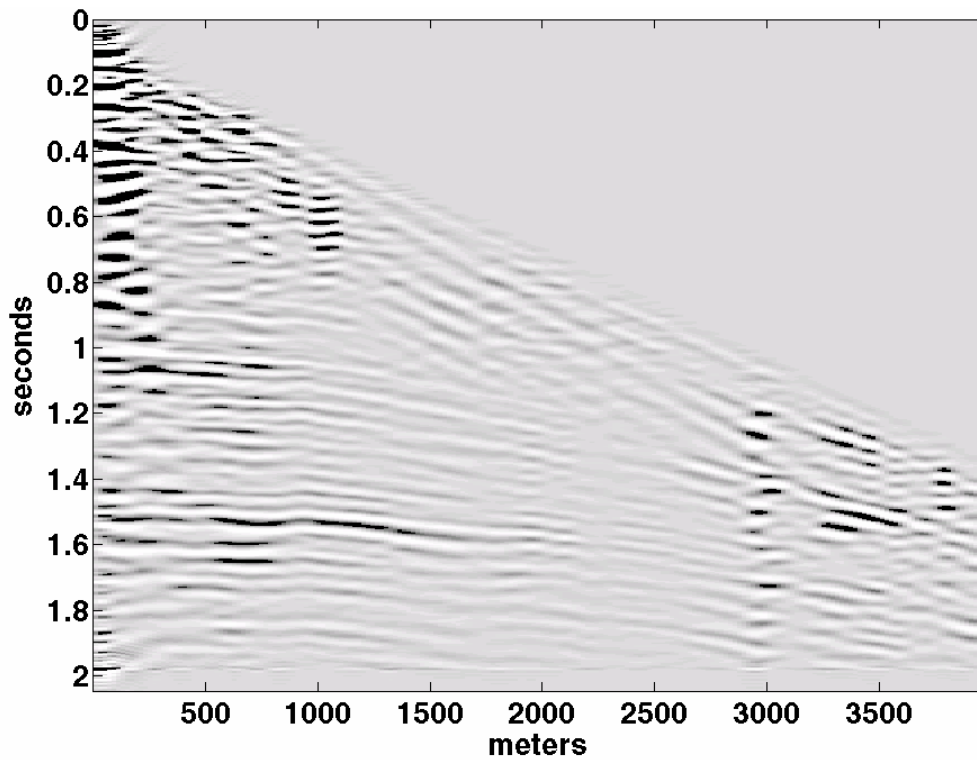


FIG. 20: The shot record of Figure 18 after 5 downward extrapolation steps of 10 m each.

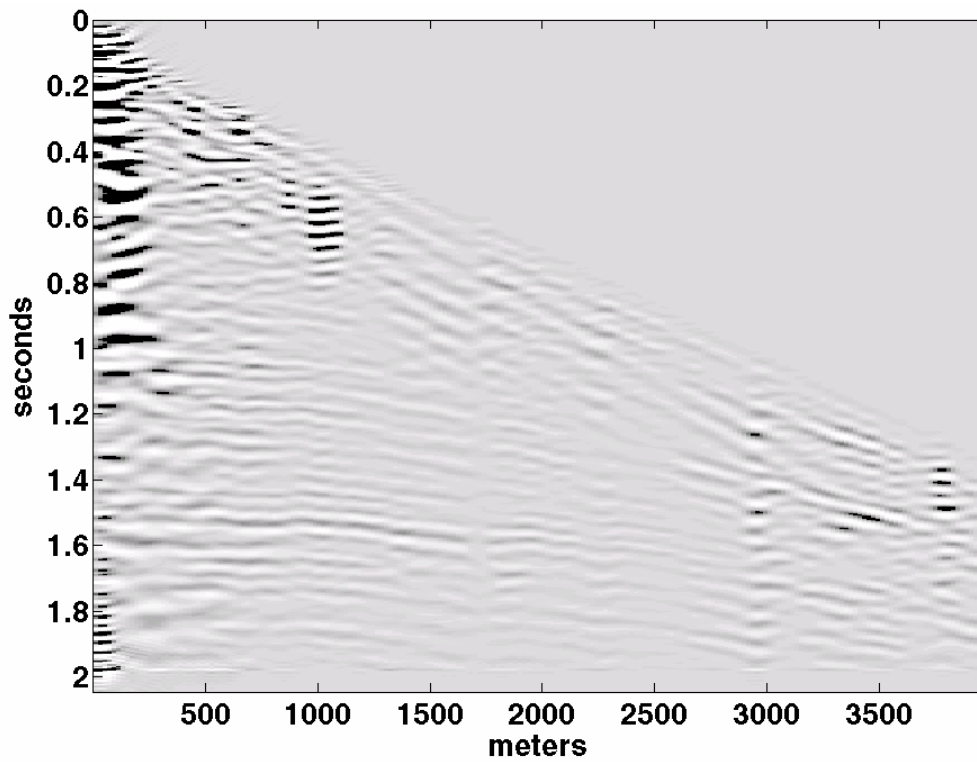


FIG. 21: The shot record of Figure 19 after 5 downward extrapolation steps of 10 m each. On the first step, the wavefield was resampled to the same number of traces as Figure 18.